12th International Conference on Fracture Mechanics of Concrete and Concrete Structures
FraMCoS-12
B.L.A. Pichler, Ch. Hellmich, P. Preinstorfer (Eds)

https://doi.org/10.21012/FC12.1252
MS02-1:1

IMPACT OF FIBER DISTRIBUTION ON FATIGUE LIFE VARIABILITY IN HIGH-PERFORMANCE FIBER-REINFORCED CONCRETE

ÁLVARO MENA-ALONSO[*], MIGUEL A. VICENTE[*], DORYS C. GONZÁLEZ[*] AND JESÚS MÍNGUEZ[*]

[*] University of Burgos, Department of Civil Engineering
Calle Villadiego s/n, 09001 Burgos, Spain
e-mail: amena@ubu.es, www.ubu.es

Key words: Fiber-reinforced concrete, flexural fatigue, fiber orientation, fatigue life, micro-CT.

Abstract: This study analyzes the influence of fiber orientation on the scatter of fatigue life in fiber-reinforced concrete (FRC). For this purpose, prismatic specimens with three fiber contents were manufactured and subsequently subjected to bending fatigue under identical relative stress levels. Fiber orientation and distribution were characterized using micro-computed tomography prior to testing. The results show that fiber orientation parameters (mean angle relative to the longitudinal axis and orientation factor along this axis) clearly correlate with fatigue life. Specimens with better-aligned fibers endured a greater number of cycles, and this relationship was observed both in the combined analysis of all series and in separate studies. Furthermore, fiber orientation affects the rate of fatigue damage propagation. These findings contribute to reducing uncertainty in fatigue tests, optimizing fatigue design criteria.

1 INTRODUCTION

The experimental study of fatigue is complex. One of its major challenges is the high variability in results in terms of fatigue life (N). When identical specimens (same geometry, mix design, and batch) are subjected to cyclic loading under the same stress levels, the number of cycles to failure often varies by two or more orders of magnitude. This uncertainty has significant implications for the structural design of elements subjected to fatigue, such as requiring numerous tests to characterize a specific type of concrete or adopting highly conservative design criteria in structural codes [1].

Many parameters affect the fatigue strength of concrete, which can be classified into three groups: load-related, material-related, and environmental. However, under fatigue tests conducted at the same stress levels, it is expected that only material-related parameters are responsible for the scatter in N. This is because load-related parameters (maximum and minimum stresses, frequency) and environmental parameters (temperature, humidity) remain constant.

Consequently, the variability in results is expected to be explained by the intrinsic heterogeneity of concrete. In other words, even with the same mix design and batch, the distribution of concrete mesostructure (aggregates, paste, pores, fibers) varies among specimens. Certain distributions of these components may better withstand cyclic loading than others. Numerous studies have investigated the influence of concrete mesostructure heterogeneity on its mechanical behavior, both under static and fatigue conditions [2–6].

In the specific case of fiber-reinforced concrete (FRC) subjected to bending, it is expected that the fibers themselves are the

dominant factor influencing fatigue strength and thus the variability in results. This is because, once the concrete matrix fractures, the primary load-bearing mechanism involves the bond forces between the fibers and the matrix. In this regard, many studies have examined the impact of fiber distribution and orientation on the static bending strength of FRC [7,8]. However, research on fatigue behavior is more limited [9,10].

The aim of this study is to investigate the variability in fatigue life of FRC under cyclic bending loads. For this purpose, three series of specimens with different steel fiber contents were manufactured and subjected to bending fatigue under identical relative stress levels. Correlations were established between fatigue performance and fiber distribution.

2 EXPERIMENTAL PROGRAM

2.1 Materials and specimens

In this study, fiber-reinforced concrete with three different fiber dosages (0.3%, 0.6%, and 1%) was used. The lowest dosage corresponds to the minimum amount recommended by the manufacturer. The concrete developed is high-strength and self-compacting, with the mixes designed to ensure that fiber content was the only variable between them.

Table 1: Mix proportions (in kg/m^3).

Component	A1	A2	A3
Cement CEM I 52.5 R	400.0		
4/10 siliceous aggregate	538.2		
0/4 siliceous aggregate	847.1		
Limestone filler	448.8		
Water	160.0		
Superplasticizer	16.0		
Nanosilica	20.0		
Steel fibers	23.6	47.1	78.5

Table 1 presents the mix proportions for the three series. The steel fibers used were Dramix RC-80/30-CP (Bekaert, Zwevegem, Belgium), featuring hooked ends, a length of 30 mm, and a thickness of 0.38 mm.

For testing, 16 prismatic specimens measuring 75 × 75 × 300 mm were cast for each series. All specimens included a central notch of 12.5 mm, maintaining a geometry scaled to that defined in the EN 14651 standard [11] for FRC flexural strength tests. The reduced size of the specimens allows for analysis via micro-computed tomography (micro-CT), as is explained below. Additionally, 8 cylindrical specimens measuring 150 × 300 mm were produced for each series for concrete mechanical characterization.

The specimens were cured for one year under controlled conditions of 20°C and 95% relative humidity. This procedure ensures that variations in concrete strength are negligible, minimizing their influence on the fatigue test results.

2.2 Material characterization

Tests were conducted to characterize both fresh and hardened concrete. In the fresh state, the tests demonstrated that all series met the self-compacting requirements. This was verified using the slump flow test [12], where the diameter of the poured concrete ranged from 770 mm (series A1) to 650 mm (series A3).

At one year of age, both compressive strength and elastic modulus were measured. The results showed an average compressive strength of 106.7 MPa and an average elastic modulus of 45.4 GPa for all series. None of these parameters showed significant variations with fiber content.

Furthermore, just before performing the fatigue tests, the concrete was subjected to three-point static bending tests [11]. The average values of the proportionality limit stress (f_{LOP}) and the residual post-cracking stress (σ_{res}) are listed in Table 2. In all cases, $\sigma_{res} > f_{LOP}$, indicating that the residual strength due to the bond between the fibers and the matrix is greater than the matrix's first crack strength (strain hardening). As expected, σ_{res} values increased as fiber content increased.

Table 2: Static bending strength. Stress levels in the bending fatigue tests.

Series	f_{LOP}	σ_{res}	$\sigma_{fat,max}$	$\sigma_{fat,min}$
A1	7.36	8.78	7.02	1.40
A2	8.35	11.78	9.42	1.88
A3	10.45	19.65	15.72	3.14

2.3 Cyclic tests

A total of 12 fatigue tests were conducted for each series, using prismatic specimens with notches and without pre-cracking. The tests involved applying load cycles with constant stress levels until specimen failure.

To determine the stress levels, the average value of the residual post-cracking stress (σ_{res}) for each series was used as a reference. The load cycles ranged from 16% to 80% of σ_{res}, ensuring that all series were subjected to the same relative stress levels, thus eliminating the effect of variations in static strength. The maximum and minimum cyclic stress values ($\sigma_{fat,max}$ and $\sigma_{fat,min}$, respectively) are listed in Table 2.

The load cycle frequency was 5 Hz. During the tests, data on load, relative displacement, and crack mouth opening displacement (CMOD) were continuously recorded.

2.4 Fiber orientation determination

To analyze the fiber distribution, the specimens were examined using micro-computed tomography (micro-CT). This technology is based on the attenuation of X-rays as they pass through matter, which depends on its density. The result of scanning a specimen is a tomogram: a set of grayscale images containing cross-sectional views of the sample at each level, where the grayscale value of each pixel corresponds to its relative density.

The potential of micro-CT lies in the post-processing of the tomograms. By applying segmentation techniques, the different components of the concrete's mesostructure (fibers, aggregates, pores) can be isolated and their individual properties (position, volume, surface area, orientations, etc.) extracted. A large body of literature exists on using micro-CT to study fiber distribution in FRC, as well as to analyze pores and crack patterns [13–17].

A CoreTOM micro-CT device, manufactured by Tescan (Brno, Czech Republic), located at the National Research Center for Human Evolution in Burgos (Spain), was used for scanning.

All specimens were scanned prior to the tests. After scanning, the micro-CT images were post-processed using the Dragonfly image analysis software from ORS (Montréal, Canada). Using advanced segmentation techniques based on convolutional neural networks (CNN), the fibers in all scanned samples were isolated, and their properties were obtained (Figure 1).

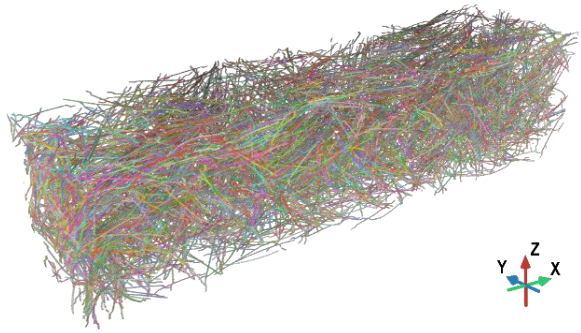

Figure 1: Fiber identification in a specimen from series A3.

3 RESULTS AND DISCUSSION

3.1 Fatigue behavior

This section presents the results of the fatigue tests. Table 3 lists the number of cycles to failure for all specimens. It is worth noting that in some tests from series A1 and A2, an initial fatigue phase was observed, of variable duration, during which the concrete matrix had not yet cracked, and therefore, no macro-crack had formed from the notch. The cycles associated with this phase were discarded, as it is assumed that the fiber intervention during this period is minimal.

Table 3 shows that all series exhibit significant variability in fatigue life, reaching up to two orders of magnitude. To facilitate interpretation, the results were fitted to a two-parameter Weibull distribution function. This probability model fits well to the statistical distribution of N in concrete fatigue.

Figure 2 shows the Weibull fits for the fatigue lives of each series. Table 4 lists the values of the fitting parameters, λ and β, as well as N for a cumulative probability of $p = 0.5$. The λ parameter is related to the characteristic fatigue life (the higher the λ, the greater the N), while β is related to the dispersion (the higher the β, the lower the variability of N).

Table 3: Fatigue life N.

A1	A2	A3
5,775	3,463	18,889
2,914	9,812	918
3,665	40,808	30
43	19,344	3,176
694	22,428	12,888
2,742	0*	7,195
7,108	26,252	15,225
3,629	20,746	12
1,495	5,156	31
4,329	5,068	3,090
1,710	14,233	3,743
48	5,024	2,219

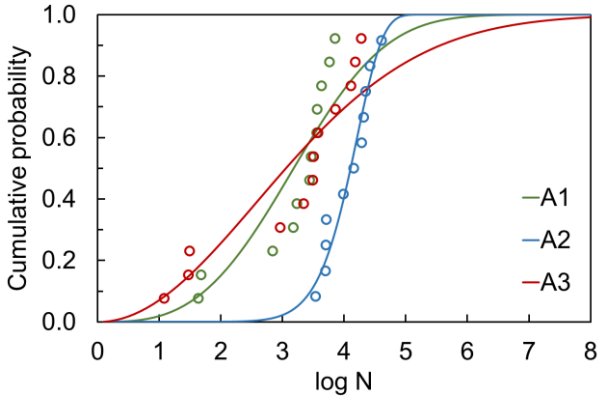

Figure 2: Weibull fits of fatigue life.

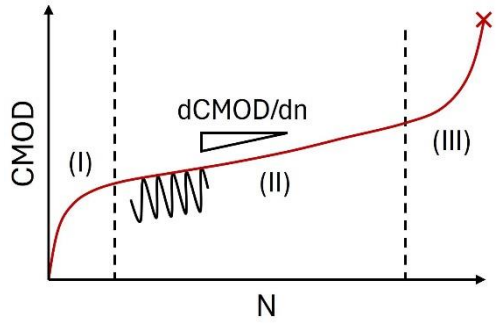

Figure 3: Fatigue creep curve.

Several interesting conclusions can be drawn from Figure 2 and Table 4. First, series A2 exhibits the longest fatigue life, as its fit curve is the furthest to the right. In contrast, series A1 and A3 show very similar statistical distributions of fatigue life. Second, there is no clear trend regarding the impact of fiber content on fatigue life; in other words, a higher fiber volume does not necessarily increase fatigue resistance. Finally, series A2 has a statistical distribution of results different from the other two series, with no tests showing N < 10^3 cycles. The variability of N is unusually low compared to typical concrete fatigue behavior.

In addition to N, fatigue creep curves, which represent the maximum CMOD at each cycle versus the number of cycles (Figure 3), were also analyzed. These curves provide information on the evolution of fatigue damage. Specifically, the notch opening rate (dCMOD/dn) was calculated, defined as the slope of the central section. This parameter is very interesting, as several studies indicate it has a strong correlation with N [18,19].

3.2 Relationship between fatigue response and fiber orientation

One of the factors that may have a significant impact on the variability of fatigue life in FRC is fiber orientation. Several parameters can be used to characterize orientation. In this study, two parameters were employed: the average angle formed by the fibers with the longitudinal axis Z ($\alpha_{Z,m}$) and the orientation factor along the longitudinal axis Z (η_Z). The latter is defined as the average projection of the unit vectors of the fibers in the Z-axis direction (Eq. (1)) [20]:

$$\eta_Z = \frac{1}{N_f}\sum_{i=1}^{N_f} \cos\alpha_Z^i \qquad (1)$$

where N_f is the number of fibers in the considered specimen volume, and α_Z^i is the angle between fiber i and the Z-axis. Therefore, η_Z takes values between 0 and 1, where 1 would indicate that all fibers are parallel to the Z-axis, and vice versa.

Given the chosen axis system for the specimens (Figure 1), only orientation parameters with respect to the longitudinal axis were calculated. This is because the Z-axis is perpendicular to the theoretical failure plane.

Another important note is that only fibers located in the central 30 mm of the specimens along the longitudinal direction were considered. This is because the failure due to bending is localized, and therefore, the fibers in this region are the ones that potentially influence the fatigue response.

Figure 4 show the relationship between the

logarithm of fatigue life and the two fiber orientation parameters ($\alpha_{Z,m}$ and η_Z, respectively), considering the results of all the series together.

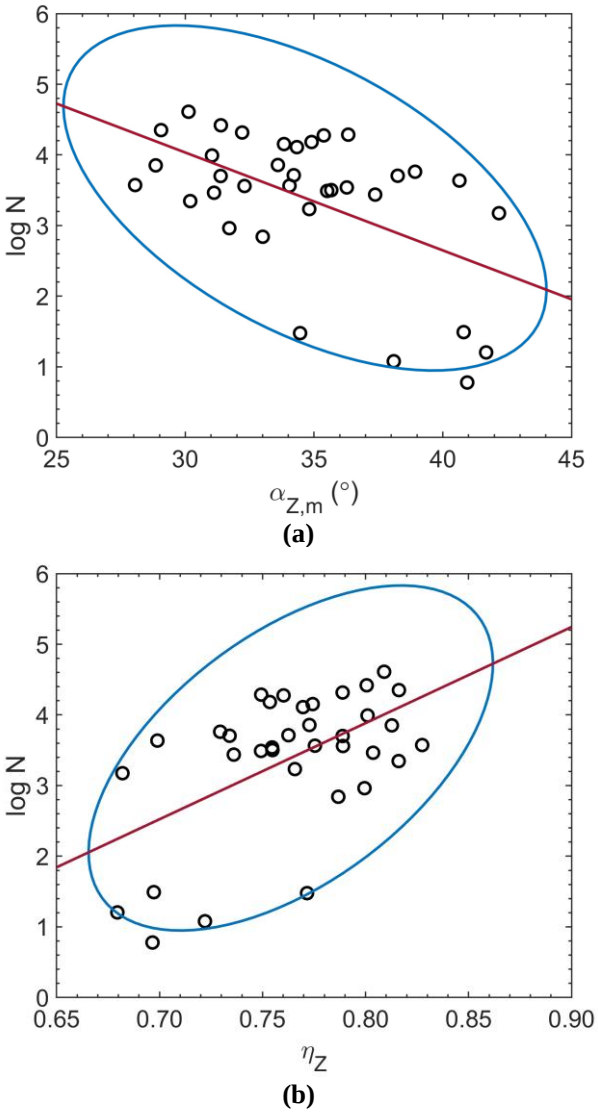

Figure 4: Relationship between log N and fiber orientation, considering all series together: (a) $\alpha_{z,m}$, (b) η_z. Confidence ellipse in blue and linear regression line in red.

To evaluate the correlation between the variables, confidence ellipses and linear regressions were used. The confidence ellipses represent regions where 95% of the data are expected to lie under the assumption of multivariate normality. These regions are constructed from the means, covariances, and critical values of the chi-squared (χ^2) distribution, allowing a clear visualization of the joint dispersion and statistical relationship between the variables. On the other hand, linear regression was used to model the functional relationship between the variables, providing a quantitative fit through a line that minimizes the mean squared error between observed and predicted values. While the confidence ellipses provide a graphical representation of the relationship and variability, linear regression quantifies the strength and direction of that relationship, thus complementing the analysis.

In Figure 4, it can be observed that, although the confidence ellipses indicate a significant dispersion of the data, both the regression line and the major axis of the ellipses suggest a clear trend. Specifically, specimens with higher values of η_Z and lower values of $\alpha_{Z,m}$ (fibers more perpendicular to the theoretical failure plane) tend to exhibit a longer fatigue life. This highlights that fiber orientation has a direct impact on the dispersion of N observed in tests of identical specimens.

In Figure 5, the relationship between the logarithm of N and fiber orientation is again shown, this time distinguishing between series. To facilitate the interpretation of the results, only the confidence ellipses are represented.

From Figure 5, several conclusions can be drawn. First, the trends indicated by the ellipses of the series are the same as the global ellipse, meaning that greater fiber alignment with respect to the Z-axis leads to a higher fatigue life. Second, the series A2 shows the best fit, as its confidence ellipse is narrower and elongated, indicating less data dispersion. It is worth noting that this series exhibited a statistically different behavior in terms of fatigue life. In contrast, series A1 and A3 present similar confidence ellipses, both in size and orientation. This indicates that the correlation between fatigue life and fiber orientation is similar in these two series. In other words, if two specimens from the same series have a certain difference in fiber orientation, their expected difference in fatigue lives will be similar.

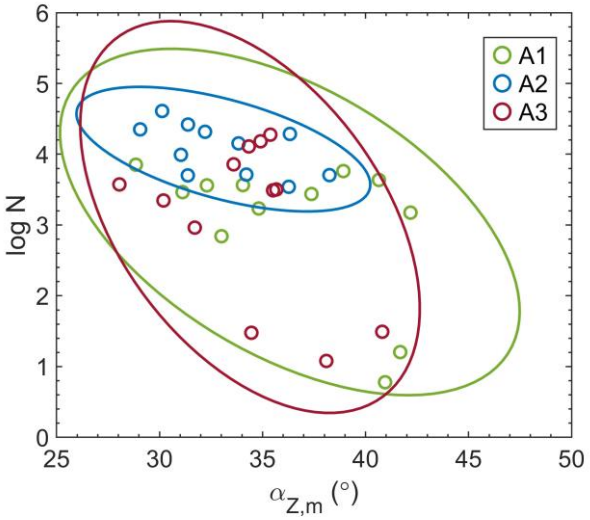

(a)

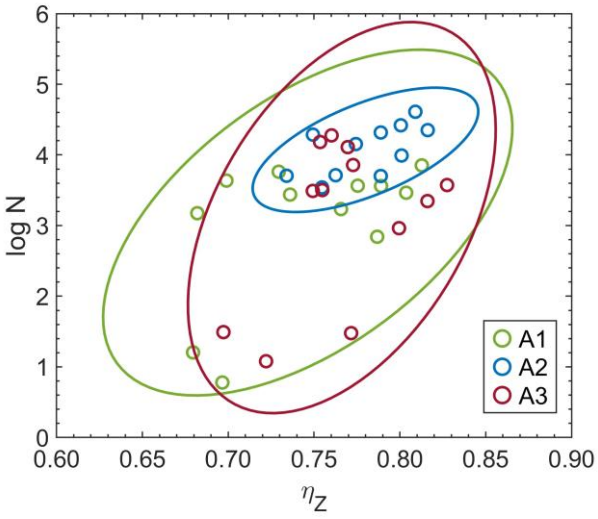

(b)

Figure 5: Relationship between log N and fiber orientation, divided by series: (a) $\alpha_{z,m}$, (b) η_z.

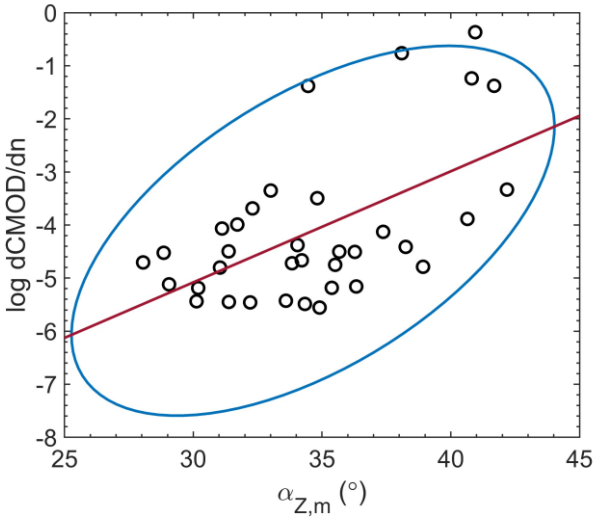

(a)

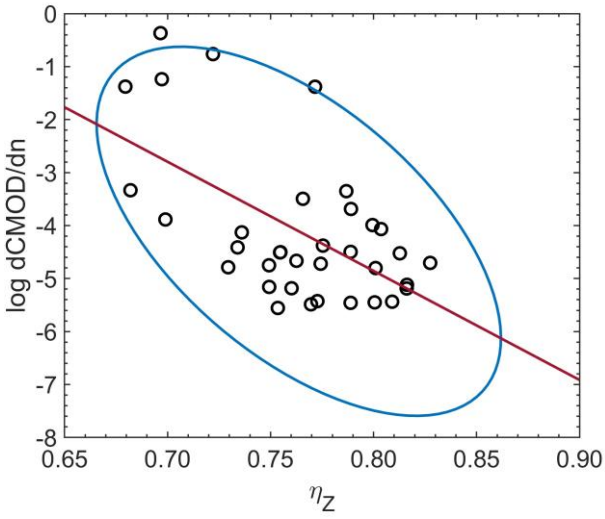

(b)

Figure 6: Relationship between dCMOD/dn and fiber orientation, considering all series together: (a) $\alpha_{Z,m}$, (b) η_Z.

On the other hand, Figure 6 presents the relationship between the logarithm of the notch opening rate dCMOD/dn and the two fiber orientation parameters, considering the data from all series together.

The results in Figure 6 indicate a clear trend between the logarithm of dCMOD/dn and fiber orientation. It can be seen that a more perpendicular fiber arrangement to the theoretical failure plane leads to a slower damage propagation rate due to fatigue. Furthermore, this correlation shows a good fit, even when considering FRC results with different fiber dosages simultaneously.

5 CONCLUSIONS

In this study, the influence of fiber distribution on the fatigue life variability of fiber-reinforced concrete (FRC) is investigated. For this, prismatic FRC specimens with three different fiber contents (0.3%, 0.6%, and 1% by volume) were fabricated and subjected to bending fatigue under the same relative stress levels. The distribution and orientation of the fibers were determined through micro-computed tomography scans before the tests. The main conclusions of the article are summarized as follows.

First, the two fiber orientation parameters

(mean angle with respect to the longitudinal axis and orientation factor along the longitudinal axis) show a clear correlation with fatigue life. Specifically, specimens with fibers better aligned with the Z-axis (higher values of $\alpha_{Z,m}$ and η_Z) can withstand a greater number of cycles, and vice versa. This is demonstrated through confidence ellipses and linear regression models.

Second, this relationship holds true both when considering all series together and when analyzing them separately. In fact, in the A1 and A3 series, which have a similar statistical distribution of N, the confidence ellipses correlating log N with the orientation parameters are similar in size and position.

Finally, it is observed that the fiber orientation also partially determines the rate at which fatigue damage propagates from the notch, as there is a good correlation of $\alpha_{Z,m}$ and η_Z with the notch opening rate dCMOD/dn.

In conclusion, determining fiber orientation parameters that correlate well with fatigue life is essential to eliminating sources of uncertainty in fatigue results. This will help optimize and improve fatigue design criteria in future standards.

REFERENCES

[1] C. Ríos, J.C. Lancha, M.Á. Vicente, Fatigue in Structural Concrete According to the New Eurocode 2, Hormigón y Acero (2023). https://doi.org/10.33586/hya.2023.3100.

[2] A.K. Chandrappa, K.P. Biligiri, Effect of pore structure on fatigue of pervious concrete, Road Materials and Pavement Design 20 (2019) 1525–1547. https://doi.org/10.1080/14680629.2018.1464500.

[3] N. Oneschkow, T. Timmermann, Influence of the composition of high-strength concrete and mortar on the compressive fatigue behaviour, Materials and Structures/Materiaux et Constructions 55 (2022). https://doi.org/10.1617/s11527-021-01868-7.

[4] M.A. Vicente, D.C. González, J. Mínguez, M.A. Tarifa, G. Ruiz, R. Hindi, Influence of the pore morphology of high strength concrete on its fatigue life, Int J Fatigue 112 (2018) 106–116. https://doi.org/10.1016/j.ijfatigue.2018.03.006.

[5] Q. Peng, L. Wang, Q. Lu, Influence of recycled coarse aggregate replacement percentage on fatigue performance of recycled aggregate concrete, Constr Build Mater 169 (2018) 347–353. https://doi.org/10.1016/j.conbuildmat.2018.02.196.

[6] S.R. Kasu, S. Deb, N. Mitra, A.R. Muppireddy, S.R. Kusam, Influence of aggregate size on flexural fatigue response of concrete, Constr Build Mater 229 (2019). https://doi.org/10.1016/j.conbuildmat.2019.116922.

[7] Ł. Skarżyński, J. Suchorzewski, Mechanical and fracture properties of concrete reinforced with recycled and industrial steel fibers using Digital Image Correlation technique and X-ray micro computed tomography, Constr Build Mater 183 (2018) 283–299. https://doi.org/10.1016/j.conbuildmat.2018.06.182.

[8] B. Zhou, Y. Uchida, Influence of flowability, casting time and formwork geometry on fiber orientation and mechanical properties of UHPFRC, Cem Concr Res 95 (2017) 164–177. https://doi.org/10.1016/j.cemconres.2017.02.017.

[9] J. Zhan, A. Nussbaumer, E. Brühwiler, Influence of fiber orientation on the high cycle tensile fatigue resistance of Ultra-High Performance Fiber Reinforced Cementitious Composites (UHPFRC), Int J Fatigue 180 (2024). https://doi.org/10.1016/j.ijfatigue.2023.108103.

[10] D.C. González, Á. Mena-Alonso, J. Mínguez, J.A. Martínez, M.A. Vicente, Effect of Fiber Orientation on the Fatigue Behavior of Steel Fiber-

Reinforced Concrete Specimens by Performing Wedge Splitting Tests and Computed Tomography Scanning, Int J Concr Struct Mater 18 (2024) 4. https://doi.org/10.1186/s40069-023-00639-8.

[11] European Committee for Standardisation (CEN), UNE-EN 14651. Test method for metallic fibre concrete. Measuring the flexural tensile strength (limit of proportionality (LOP), residual), 2008.

[12] UNE-EN 12350-8. Testing fresh concrete. Part 8: Self-compacting concrete. Slump-flow test, 2011.

[13] M.A. Vicente, G. Ruiz, D.C. González, J. Mínguez, M. Tarifa, X. Zhang, CT-Scan study of crack patterns of fiber-reinforced concrete loaded monotonically and under low-cycle fatigue, Int J Fatigue 114 (2018) 138–147. https://doi.org/10.1016/j.ijfatigue.2018.05.011.

[14] T. Oesch, E. Landis, D. Kuchma, A methodology for quantifying the impact of casting procedure on anisotropy in fiber-reinforced concrete using X-ray CT, Materials and Structures/Materiaux et Constructions 51 (2018). https://doi.org/10.1617/s11527-018-1198-8.

[15] M.A. Vicente, G. Ruiz, D.C. González, J. Mínguez, M. Tarifa, X. Zhang, Effects of fiber orientation and content on the static and fatigue behavior of SFRC by using CT-Scan technology, Int J Fatigue 128 (2019) 105178. https://doi.org/10.1016/j.ijfatigue.2019.06.038.

[16] Y. Zhao, X. Wang, J. Jiang, L. Zhou, Characterization of interconnectivity, size distribution and uniformity of air voids in porous asphalt concrete using X-ray CT scanning images, Constr Build Mater 213 (2019) 182–193. https://doi.org/10.1016/j.conbuildmat.2019.04.056.

[17] Skarżyński, J. Tejchman, Experimental investigations of damage evolution in concrete during bending by continuous micro-CT scanning, Mater Charact 154 (2019) 40–52. https://doi.org/10.1016/j.matchar.2019.05.034.

[18] D.M. Carlesso, A. de la Fuente, S.H.P. Cavalaro, Fatigue of cracked high performance fiber reinforced concrete subjected to bending, Constr Build Mater 220 (2019) 444–455. https://doi.org/10.1016/j.conbuildmat.2019.06.038.

[19] F. Germano, G. Tiberti, G. Plizzari, Post-peak fatigue performance of steel fiber reinforced concrete under flexure, Materials and Structures/Materiaux et Constructions 49 (2016) 4229–4245. https://doi.org/10.1617/s11527-015-0783-3.

[20] F. Laranjeira, S. Grünewald, J. Walraven, C. Blom, C. Molins, A. Aguado, Characterization of the orientation profile of steel fiber reinforced concrete, Materials and Structures/Materiaux et Constructions 44 (2011) 1093–1111. https://doi.org/10.1617/s11527-010-9686-5.